J Electroceram (2010) 25:99–107
DOI 10.1007/s10832-009-9596-5

Ion transport studies on Al–Zn ferrite dispersed nano-composite polymer electrolyte

Kamlesh Pandey · Mrigank Mauli Dwivedi · I. M. L. Das · Markandey Singh · Shankar Lal Agrawal

Received: 3 August 2009 / Accepted: 22 December 2009 / Published online: 20 January 2010

Abstract A ferrite dispersed PEO based nano-composite polymer electrolyte has been developed in the present work. Formation of nano-composites, change in the structural and microscopic properties of the system have been investigated by X-ray diffraction, optical microscopy and SEM imaging. Existence of spinodal decomposition structure indicates formation of nano sized composite polymer electrolyte. Increase in formation of crystalline domain has been evidenced in thermal studies upon dispersal of nano-sized filler particles in pristine electrolyte matrix. The ionic transport studies through impedance spectroscopy exhibit highest electrical conductivity for the composition [93PEO-7NH_4SCN]: 2 wt% Al–Zn ferrite, viz. is 1.22×10^{-4} S/cm at room temperature with ionic transference number in excess of 0.9. Arrhenius type thermally activated conduction process is reflected during temperature dependent conductivity studies on these electrolytes.

K. Pandey (✉) · M. M. Dwivedi
National Centre of Experimental Mineralogy and Petrology,
University of Allahabad,
Allahabad, India
e-mail: kp542831@gmail.com

M. M. Dwivedi
e-mail: MMDwivedi@gmail.com

I. M. L. Das
Department of Physics, University of Allahabad,
Allahabad, India

M. Singh · S. L. Agrawal
Department of Physics, A. P. S. University,
Rewa, M. P., India

S. L. Agrawal
e-mail: sla_ssi@rediffmail.com

Keywords Nano-composite polymer electrolyte · Polymer electrolyte · Nano-composite electrolyte · Al–Zn Ferrite · Electrical conductivity · Spinodal structure

1 Introduction

In recent years, materials with nano scale microstructure, i.e. nano crystalline materials or nano-composites, are increasingly becoming important for their technological importance due to their unique electrical, magnetic and optical properties. In this context, composite polymer electrolytes in general and nano-composite polymer electrolytes in particular have been extensively studied for electrochemical applications over the years due to the possibility of achieving better ionic conductivity [1–4]. Usually in composite polymer electrolytes (CPE), an inorganic/ceramic, ferro-electric [5–9] or high molecular weight organic filler [10, 11] is dispersed in the polymer electrolyte matrix as a third component, which improves the mechanical, electrical and optical properties.

Ferrite is yet another class of material which is usually characterized by high dielectric constant (relative permittivity) and high relative permeability (μ_r) below Curie temperature. Spinel ferrites are extremely important for academic and technological applications. In particular, ferrite nanoparticles can be used in magnetic drug targeting, tissue engineering, biological high gradient magnetic selective separation for cell sorting, DNA isolation, magnetic resonance imaging contrast agents and hyperthermia. The multifunctional response of these materials can have tremendous potential and lead to improved materials for applications like magneto resistive damping, mechanical and electrical devices: loudspeakers, seals, sensors, dampers, etc. [12–14]. The physical properties of spinel ferrite

such as electrical, magnetic and elastic properties are governed by the type of magnetic ions residing on the tetrahedral (A) and octahedral (B) sites in the crystal lattice [15–18] and the relative strength of the inter and intra sublattice interaction [19]. Ferrite-based materials have excellent chemical stability and are relatively cheap to produce. The Polymer ferrite nano-composite films have high magneto-electronic sensitivity due to large magnetisation of filler materials. Such polymer magnets have been widely used in various fields, e.g. electronic and communications instruments, household tools, and audio equipments [20, 21]. These properties of ferrites thus makes them a potent filler material for development of nano-composites for electrochemical applications especially PEM fuel cells and controlled drug delivery system [22].In one of the two approaches used in drug delivery design, system responds to change in local environment thereby changing the rate of drug delivery. In this respect, ferrite based nanocomposite electrolytes are expected to respond to stimuli like magnetic field and electric field and thus help in drug delivery [23]. Likewise ferrite fillers based polymer electrolytes are expected to provide a mechanically stable highly conducting electrolyte for PEM fuel cell applications [24].

Prompted by these considerations we have investigated the structure and transport properties of nano size Al–Zn ferrite dispersed proton conducting polymer composite electrolyte (PEO : NH_4SCN : Al–Zn ferrite system) and report the findings in this paper. The nano sized ferrite material has been prepared by soft chemical method (sol-gel technique). Morphological and structural studies on CPE have been carried out by optical microscopy, SEM, DSC and X-Ray diffraction (XRD). The electrical conductivity of the electrolyte was evaluated from impedance spectroscopic technique.

2 Experimental

PEO based nano-composite films were prepared by standard solution cast technique. Commercial Polyethylene oxide (ACROS, M.W. 6×10^5) was used as a host polymer matrix. Ammonium thiocynate salt dissolved in D.I. water was admixed in a proper stiochiometric composition in polymer. Thereafter the synthesized nano sized Al–Zn ferrite powder was dispersed in this solution as filler. This solution, after stirring thoroughly for 10 h was casted in polypropylene dishes and allowed to evaporate slowly at room temperature (~25°C) followed by vacuum drying for 3–4 h. The nano size ferrite powder [$Al_{0.15}Zn_{0.25}(Fe_2O_4)_{0.60}$] was synthesized following wet chemistry route in which precursors Al, Zn and Fe nitrates were dissolved in water/ethanol mixture followed by addition of tetraethoxysilane (TEOS) drop by drop while stirring it at room temperature for 15 min in the molar ratio EtOH : TEOS : H_2O=3:1:10. The pH of solution was fixed within 2–3 range. The sols were allowed to gel at 40°C. After gellification it was kept for drying at 150°C for 50 h. Subsequently, the powdered gels were subjected to thermal treatment at 700°C (for 3 h) and 1000°C (for 2 h) in a Kenthal high temperature furnace. The dried material was crushed to obtain fine powder of ferrite.

XRD patterns of the ferrite powder and composite polymer electrolyte films were taken using a Phillips X'Pert X-Ray diffractometer. The diffraction pattern was recorded at room temperature using Cu K_α radiation (λ=1.542 Å) for Bragg's angle varying from 15° to 60°.The crystallite size determination and nanocomposite formation was carried out through the XRD pattern. Optical micrographs of different compositions of composite polymer electrolyte were taken using Lica make optical microscope. SEM images were taken on Joel JXA 8100 EPMA. For SEM pictures a very thin layer of carbon coating on ferrite pellet and CPE films was used. The Infrared (IR) spectrum of the CPE was taken on Perkin Elmer make IR spectrophotometer with a wave number resolution of 5 cm^{-1} in the frequency range from 4000 to 400 cm^{-1}. DSC data were collected on a Perkin Elmer DSC unit in the temperature range RT to 200°C at a heating rate of 5°C/min under N_2 atmosphere to access thermal behaviour of ferrites and composite polymer electrolyte films. The electrolyte was electrically characterized by impedance spectroscopy (using Platinum electrodes for electrical contact) in the frequency range 40 Hz-100 KHz (applied field 20 mV) using Hoiki LCZ tester (model −3520).

3 Result and discussion

3.1 Structural and thermal studies

XRD pattern of [(100×) PEO-xNH_4SCN]: 2 wt% Al–Zn ferrite and [93 PEO-7NH_4SCN]: x% Al–Zn ferrite were recorded and shown in Fig. 1(a) and (b) respectively. The X-ray diffraction pattern show change in amorphosity of polymer electrolyte after the addition of salt and ferrite filler. Peaks of Al–Zn ferrite are situated at Bragg angles 29.9° (111), 35.3° (220), 37.3° (311) and 45° (400). A comparative look of XRD peaks at variable salt or ferrite content indicates that main crystalline peaks of PEO at 19° and 23° are slightly shifted. The change in intensity of PEO related peaks along with presence of few new peaks in XRD profile of composite electrolyte essentially result from the interaction of polymeric chain with salt or filler, that increases the interlayer spacing (shown in the inset of Fig. 1(a)). In inset, some new peaks appeared at 2θ=19.1 (Al_2O_3), 22.9 (Al–Fe oxide), 23.17 (Fe_2O_3), 23.21, 23.67 and 23.81 (ZnSCN) in composite electrolyte. The increase in intensity of peaks give the information related to the interaction of PEO-salt

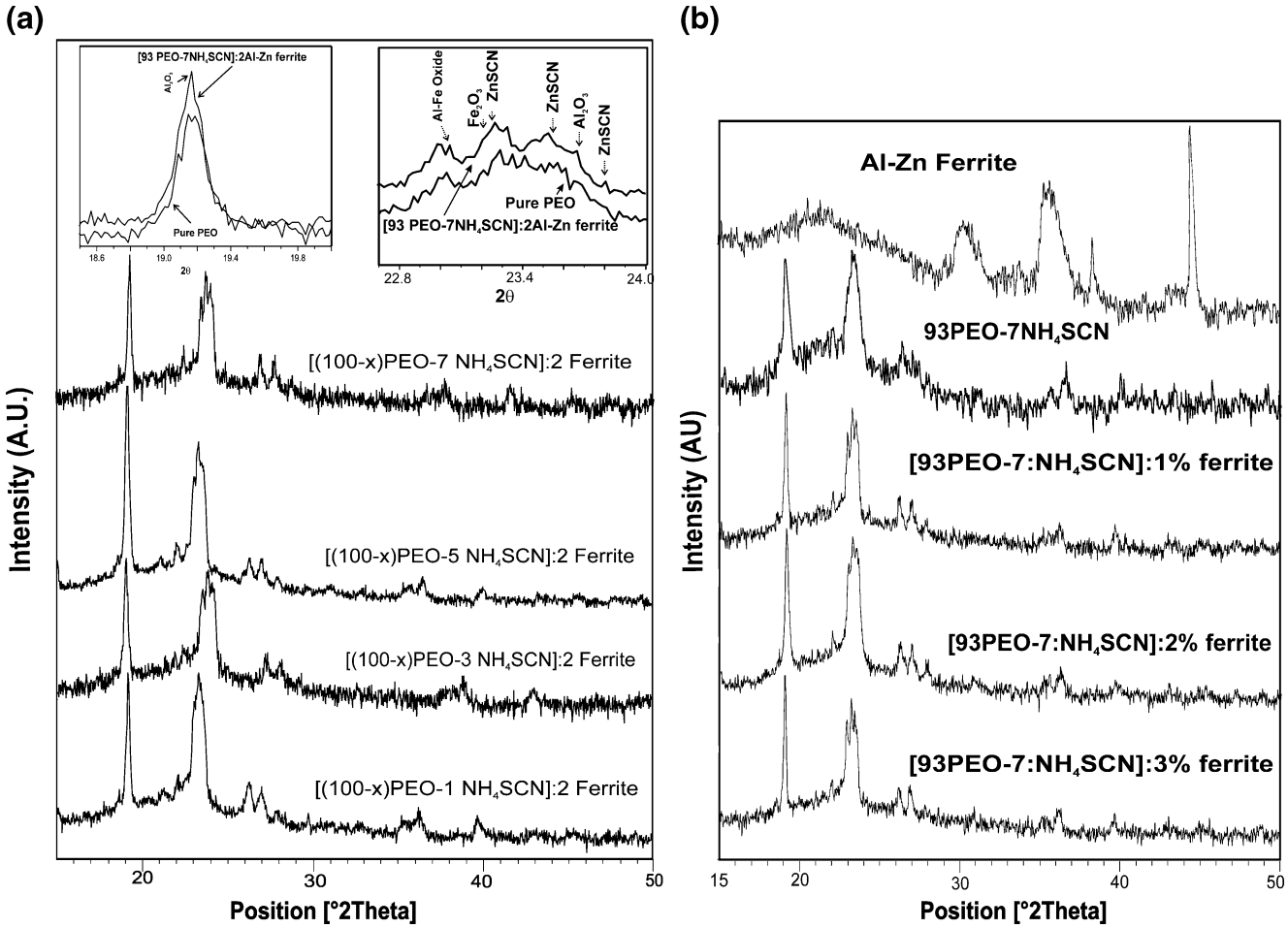

Fig. 1 (**a**) XRD pattern of {(100×) PEO-x NH_4SCN}:2% Al–Zn ferrite film. Details of the peak at 19° and 23° is given in inset. (**b**) XRD pattern of Al–Zn ferrite, 93PEO-7 $NH_4SCN$and {93PEO-7 NH_4SCN}:x% Al–Zn ferrite (where x=1, 2 and 3) film

and PEO-salt-filler. This also indicates about the composite nature of the electrolyte. The broadening in PEO peaks is possibly due to incorporation of Al (2θ=23.7°) and Fe (2θ=23.17°) in the polymeric lattice. Addition of salt and filler causes a small shift in original position of PEO peaks towards lower 2θ side along with reduction in peak intensity. No new prominent peak appears after the composite formation. The average crystallite size in CPE was calculated using the Sherrer's formula [25] and found to be 40–60 nm. In order to distinguish the effect of crystallite size induced broadening and strain induced broadening in FWHM (full width at half maxima) of XRD profile, Williamson-Hall plot method [26] was adopted. Using Williamson Hall plot (Fig. 2), crystallite size strain can be obtained from the following relation

$$\mathrm{B\,Cos}\theta = \frac{C\lambda}{t} + 2\varepsilon Sin\theta \qquad (1)$$

where B is FWHM and t the grain size (nm), C the correction factor, ε the strain and λ the wavelength of X-rays. The estimated grain size and strain for different composition of electrolytes is given in Table 1. The calculated crystallite size of sol gel synthesized Al–Zn ferrite is ~18 nm while in different CPE films it remains in between 40 and 60 nm.

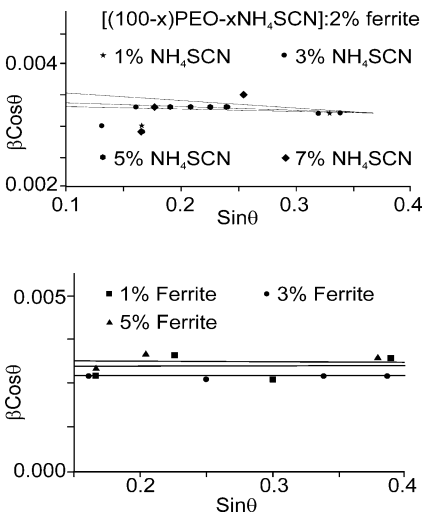

Fig. 2 Williamson-Hall plots for different polymeric film

Table 1 Calculated particle size in CPE by XRD study.

Sample Composition	Calculated crystallite size (in nm)		Av. Strain ($\times 10^{-4}$)
	Sherrer's formula	W-H plot	
1. Al–Zn ferrite	46	18	4.8
2. [99PEO-1NH_4SCN]:2 ferrite	79	44	2.3
3. [97PEO-3NH_4SCN]:2 ferrite	76	42	1.3
4. [95PEO-5NH_4SCN]:2 ferrite	77	42	2.1
5. [93PEO-7NH_4SCN]:2 ferrite	68	39	1.4
6. [93PEO-7NH_4SCN]:1 ferrite	56	51	1.7
7. [93PEO-7NH_4SCN]:3 ferrite	72	56	1.0
8. [93PEO-7NH_4SCN]:5 ferrite	68	51	8.9

The optical micrograph of {PEO–NH_4SCN}: Al–Zn ferrite system is shown in Fig. 3. In polymeric materials, two mechanism of phase separation are known "nucleation & growth" and "spinodal decomposition" [27]. The first process starts with formation of nuclei of a new component whereas in spinodal decomposition the system behaves differently. Spinodal decomposition structure is a stable structure at room temperature [28]. Optical micrographs of {PEO–NH_4SCN}: Al–Zn ferrite system ascertain presence of spinodal decomposition structure. Similarly, SEM structure of different compositions of salt and ferrite (Fig. 4(a) and (b)) affirms optical microscopy results. Spinodal decomposition process, which influences the morphology of the sample, determines its physical and chemical properties with the control of degree of dispersion. A polymer matrix being a visco-elastic system has a very wide time visco-elastic relaxation spectrum ranging from one to several decade order. The design of block chain structure of polymer and its crystallization provides the basic information regarding the formation of such a phase separation structure. Hence the formation of new patterns due to addition of salt (NH_4SCN) and filler (Al–Zn ferrite) in the PEO matrix are closely related to the backbone or chain structure of the polymer [29, 30]. The possibility of spinodal decomposition in Al–Fe system was first suggested by Munster and Sagel [31]. This is also likely to affect the morphology of CPE as has been observed in present investigations. In optical image it is very clear that a small droplet of minor phase is dispersed throughout the major phase. The host PEO has the lamellar structure. After doping of salt and dispersion of filler this lamellar structure become unstable and new patterning takes place in the plane of film. There is likely to be preferential segregation of one component on the surface but the dominant effect will be lateral phase separation. Higher ratio of doping produces unstable films reflecting the increased role of immiscibility between salt/filler and polymer matrix. In the SEM image, the heterogeneous nature of the electrolyte appears. The addition of salt and filler in the PEO matrix disturbs the original structure of the polymer. Higher content of NH_4SCN completely breaks the lameller structure and produces a spinodal structure. Similar effects are also observed in the case of films with higher ferrite ratios. These results clearly indicate strong role of filler in controlling the morphology of composite polymer electrolytes.

Infrared spectra of PEO, NH_4SCN, Al–Zn ferrite, {93PEO-7 NH_4SCN}:2 wt% Al–Zn ferrite films are depicted in Fig. 5. The IR peak assignments of these samples are given in Table 2. From the table it is clear that interaction of polymer chain with Al, Zn, and Fe ions has taken place. This result supports XRD findings (Figs. 1 and 2). The other main feature of PEO: NH_4SCN complexation is the NH_4^+ peak shift from 3149 cm^{-1} to higher wave number side at ~3200 cm^{-1}. Three strong and intense peaks (~2050 cm^{-1}, 1406 cm^{-1} and 780 cm^{-1}) have been visualized in ammonium thiocynate and attributed to the absorption frequency υ_{CN}, characteristic peak of NH_4SCN and υ_{CS} (N-bonding mode) respectively. These peaks seem to weaken upon interaction with polymer and as well as shift in the IR spectrum of composite system. Other peaks at 950 cm^{-1} and 700 cm^{-1} related to 2δ(SCN) and υ_{CS} (S-bonding) modes in NH_4SCN also change [32, 33]. In composite electrolyte the appearance of peak at 1100 cm^{-1} and 955 cm^{-1} gives an indication of C-O-C stretching vibrations [34].

No new peak appears but intensities of some existing peaks changes after complexation. The existence of peaks around 3000–3100 cm^{-1} and at 1700 cm^{-1}, 1410 cm^{-1}, 1390 cm^{-1} are related to C–H stretching, C–H in plane bending, C–O stretching and υ CH_2–O respectively. The introduction of Al–Zn ferrite in PEO: NH_4SCN system

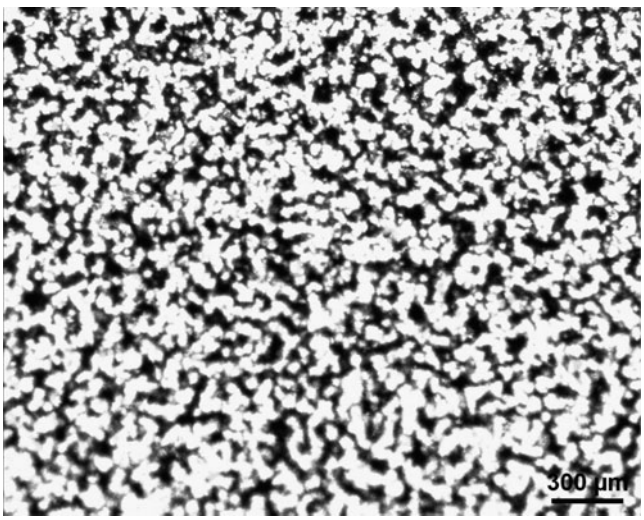

Fig. 3 Spinodal structure of {PEO-NH_4SCN}: Al–Zn ferrite system recorded by optical microscope

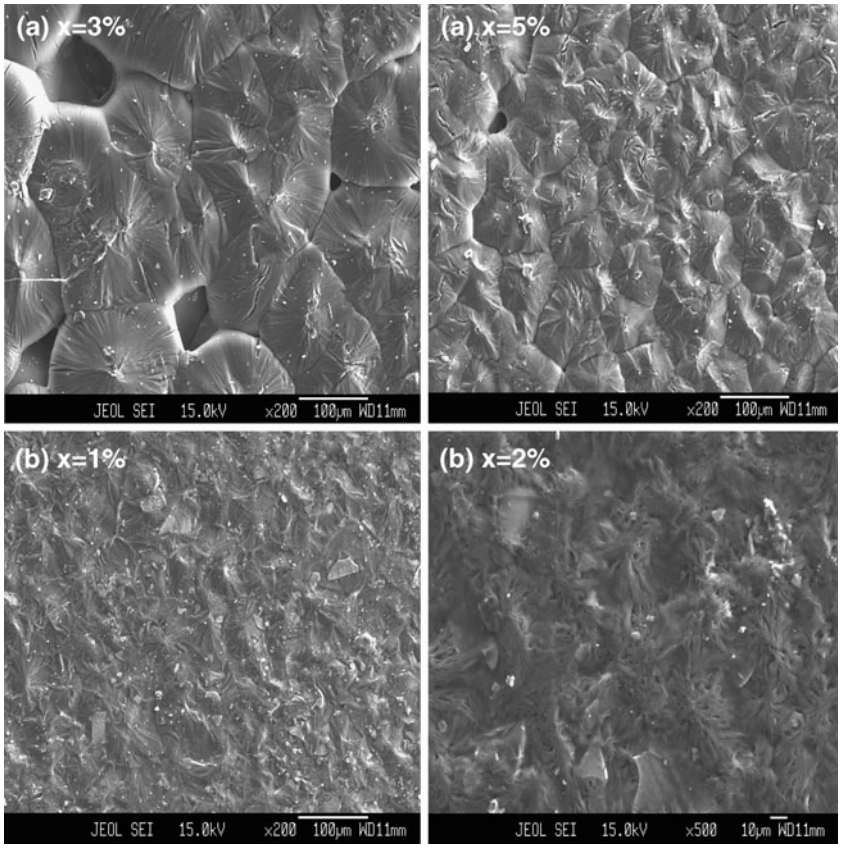

Fig. 4 SEM image of (**a**) [(1-x) PEO-x NH_4SCN]: 2% Al–Zn ferrite film and (**b**) [93PEO-7 NH_4SCN]: x% Al–Zn ferrite film

indicates the increase in amorphosity (change in bond intensity). Other feature of IR is that ferrite peak at 860 cm^{-1} in after complexation became sharper (broadening reduced). All other peaks are present in their original position with only minor change in intensities.

In the ferrite system, metal ions are situated in two sub lattice designated tetrahedral (A- site) and octahedral (B-site) according to the geometrical configuration of the oxygen nearest neighbor. Waldron [35] and Hafner [36] have attributed the band around 600 cm^{-1}, υ_1 to stretching vibration of tetrahedral group Fe^{2+}–O^{2-} and around 400 cm^{-1} to the octahedral group (υ_2). The force constant of A and B sites correspond to values reported earlier [37]. Similar observations have been recorded in the present work as well. The minor shift in υ_1 mode related ferrite peak in composite system may be possibly due to interaction of filler particles with pristine electrolyte system.

The DSC curve of pure PEO, PEO–NH_4SCN, Al–Zn ferrite alongwith [93PEO-7NH_4SCN]: 2 wt% Al–Zn ferrite are shown in Fig. 6. In pure Polyethylene oxide one endothermic peak around 68°C and one exothermic peak at 105°C are observed. The endothermic peak is due to melting of pure PEO, while the exothermic is on account of evaporation of absorbed water. Beyond 125°C PEO starts dissociating in consonance with earlier findings [7]. In DSC studies of Al–Zn ferrite, a small endothermic peak appears at ~50°C which is possibly due to the removal of absorbed humidity at low temperature. Thereafter, the filler material shows a better stability up to 200°C. The addition of salt in host polymer shifted the melting temperature of PEO to lower side (i.e. from 68°C to 52°C in 93PEO-7NH_4SCN film). It also reduced the crystallinity of the

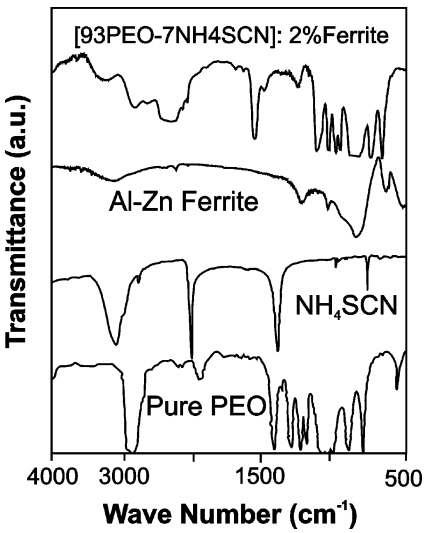

Fig. 5 IR spectra of PEO, NH_4SCN, Al–Zn ferrite and [93PEO-7 NH_4SCN]: 2% Al–Zn ferrite film

Table 2 Assignment of IR peaks of different samples.

PEO	NH_4SCN	Al–Zn Ferrite	Composite film	Assignments
		3300 cm^{-1}	3436 cm^{-1}	-OH stretching
	3149 cm^{-1}		3196 cm^{-1}	-N-H stretching in NH_4^+
2239 cm^{-1}			2239 cm^{-1}	-C-C stretching in PEO
	2169 cm^{-1}		2169 cm^{-1}	-characteristic peak of NH_4SCN
	1425 cm^{-1}		1466 cm^{-1}	-OH-CH_3 bending
1410 cm^{-1}				-C-H in plane bending
1354 cm^{-1}		1360 cm^{-1}	1354 cm^{-1}	-C-H wagging mode
				-NO_3 stretching vibration
1290 cm^{-1}		1280 cm^{-1}	1290 cm^{-1}	-Zn-O Peak
			1239 cm^{-1}	-Zn-CH_3 asymmetric deformation
1149, 1109, 1061 cm^{-1}		1084 cm^{-1}	1099 cm^{-1}	-PEO characteristic triplet, Al–O–Al, Al–CH_3 deformation
963 cm^{-1}		963 cm^{-1}	963 cm^{-1}	-SiO_2, C–CH_3 bending
	845 cm^{-1}		845 cm^{-1}	-characteristic peak of NH_4SCN
	676 cm^{-1}			-characteristic peak of NH_4SCN
		615 cm^{-1}	624 cm^{-1}	-υ_1 mode of ferrite

polymer. The addition of ferrite filler to polymer salt complex slightly enhanced the melting temperature (52°C to 63°C). It also increases the sharpness of crystalline peak or reduction in peak broadening with respect to T_m peak in DSC profile of PEO: NH_4SCN complex. This shows a slight increase in crystallinity of nano-composite material but crystilinity is still lower than that of pure PEO as indicated by the enthalpy change. This is due to the increase in formation of crystalline domain after the dispersion of ferrite filler which is likely due to interaction of polymer salt matrix with Al–Zn filler (indicated by peak shift in ferrite spectrum to higher wave number in IR studies and as well as XRD studies). The increase of crystalline domain is also responsible for the higher ionic mobility in the composite electrolyte beyond the melting temperature. The change of crystallinity and crystallite size after dispersal of Al–Zn filler in pristine electrolyte has also been noticed in XRD measurements (Table 1).

3.2 Ion transport studies

The total ionic transference number of the polymer nano-composite film has been evaluated by Wagner's polarization technique. The calculated value of t_{ion} is more than 0.84 for different polymer composite electrolytes. In PEO–NH_4SCN polymer electrolyte the ionic conductivity is mainly due to the H^+ ion. The contribution of H^+ ion has been evidenced by gas chromatography after the Coulometric experiment of pristine and as well as composite electrolyte film. This implies that the electrolytes are basically proton conducting system with a small anionic contribution to charge transport (i.e. t_{SCN^-}=0.16).

The change in bulk electrical conductivity of polymer nano-composite film as a function of salt (NH_4SCN) and filler content at different frequencies is given in Fig. 7(a) and (b) respectively. With the addition of salt/ filler an increase in the electrical conductivity is observed. The conductivity increases with salt concentration (at fixed ferrite content) up to 7–8% and thereafter it starts decreasing. Beyond this salt concentration films become fully sticky and are very difficult to handle for further measurements. Similarly, it shows a maxima at 2 wt% of ferrite (Fig. 7(b)) in the composite after which a decrease in conductivity has been observed. The increase in conduc-

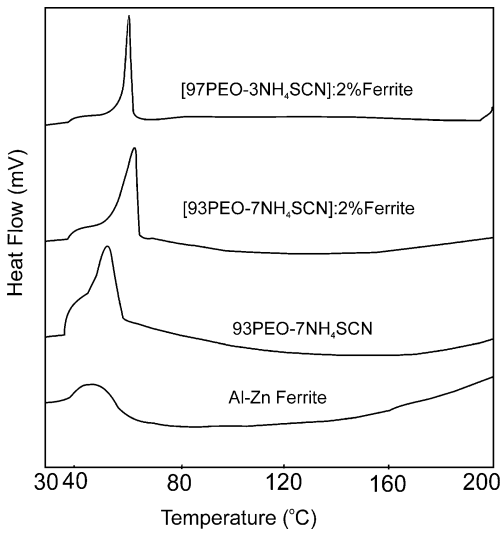

Fig. 6 DSC curve for (93PEO-7 NH_4SCN) film, Al–Zn ferrite and {[(1-x) PEO+ xNH_4SCN]-2% Al–Zn ferrite} film

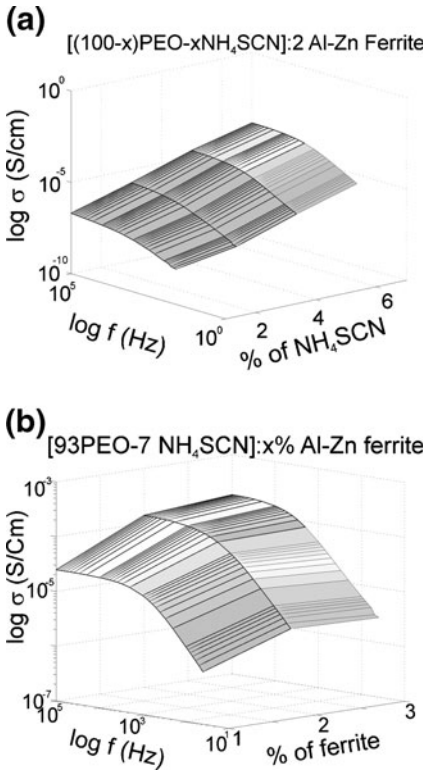

Fig. 7 Variation of conductivity with (**a**) NH_4SCN and (**b**) Al–Zn ferrite composition

tivity with salt concentration is attributed to the increase in number of charge carriers and amorphosity of the system [38, 39]. In amorphous state the molecular packing is loose and weak. Thus, the polymer chain in this phase is more flexible and capable of orienting themselves relatively easily and rapidly. The increase in salt concentration provides higher number of mobile charge carriers which is responsible for fast segmental motion. The fast segmental motion of polymeric chain reduces the relaxation time and increases ion transport properties.

A.C. conductivity, σ_{ac} of the electrolyte system has been obtained from the data on dielectric constant (ε') and loss tan δ using the relation:

$$\sigma_{ac} = \varepsilon' \varepsilon_o \ \omega \tan \delta \tag{2}$$

where ε_o is the vacuum permittivity and ω the angular frequency. The variation of a.c. conductivity for different NH_4SCN compositions in [(100×) PEO+xNH_4SCN]:2 wt% ferrite electrolyte with frequency at room temperature is shown in Fig. 8(a). The conductivity in all compositions increases with applied frequency. The ac conductivity pattern shows a small plateau in the higher frequency region. This means charge carriers are not sufficiently free to follow the changing electric field and therefore conductivity remains nearly frequency independent. The frequency dependent conductivity in nano-composite polymer electrolyte seems to follow a universal power law where the frequency dependent conductivity in solid polymer electrolyte is described by the relation [40, 41].

$$\sigma_{ac} = \sigma_0 + A\ \omega^n \tag{3}$$

where σ_0 is the dc conductivity (the extrapolation of the plateau region to zero frequency gives the value of d.c. ionic conductivity), A the pre-exponential factor and n the fraction exponent lying between 0 and 1. The calculated values of curve fitting parameters for the best conducting composite electrolyte i.e. [93PEO+7NH_4SCN]:2 wt% ferrite composition are $\sigma_0 = 1.4\times10^{-4}$ S/cm, $A = 4\times10^{-5}$ and $n = 0.74$. Generally for ionic conductors power law exponents (n) can be between 1.0–0.5, indicating the ideal long range

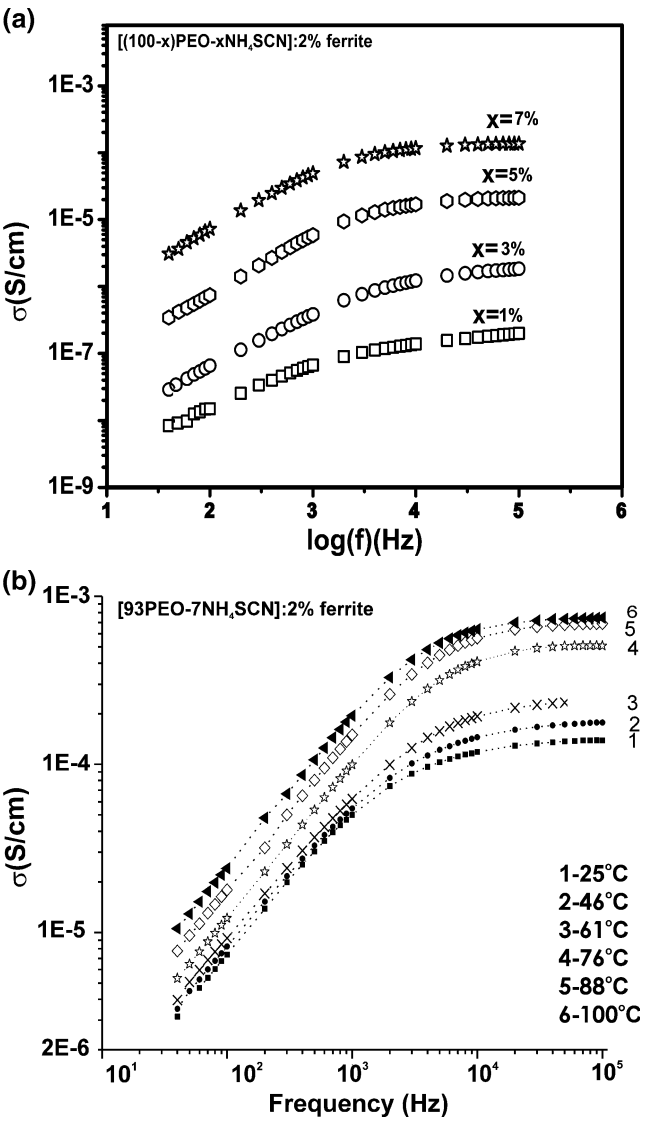

Fig. 8 (**a**) Variation of ac conductivity with frequency for different composition of nano polymer composite electrolytes at ambient temperature. (**b**) Variation of ac conductivity with frequency for [93PEO-7 NH_4SCN]: 2% Al–Zn ferrite at different temperature

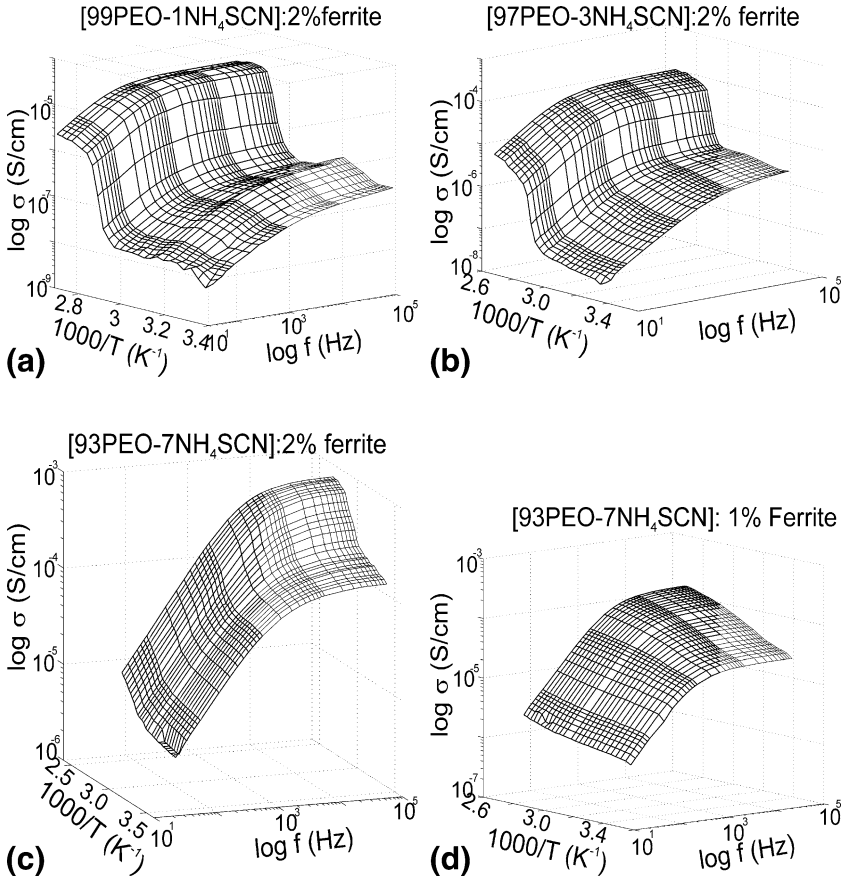

Fig. 9 Temperature dependence of conductivity for different composition of nano polymer composite electrolytes

pathway and diffusion limited hopping (tortuous pathway) respectively [42]. The change of a.c. conductivity with frequency at different temperature (RT- 100°C) for [93PEO+ 7NH_4SCN]:2 wt% ferrite film is given in Fig. 8(b). The conductivity of the film increases with increasing frequency at each temperature. At lower frequency the increase is less prominent than at higher frequency.

In Fig. 9, the variation of σ_{ac} with frequency and temperature for different nano-composite films are presented. With increasing salt content the peak height is seen to reduce with temperature. For 7% NH_4SCN composition the peak height becomes very small and conductivity value becomes 1.2×10^{-4} S.cm^{-1} at RT and 8.9×10^{-4} S.cm^{-1} at 100°C. This behavior can be explained in terms of small polaron tunneling or hopping mechanism. Small polarons are generally assumed to be localized so that their distortion clouds do not overlap. In this case the activation energy for polaron transfer (W_H) ; W_H=W_p/2, where W_p is the polaron energy ; is independent of the interstice separation. The tunneling distance (R) at a frequency (ω) is given by [43]:

$$R = \frac{1}{2\alpha}\left[\ln\frac{1}{\omega\tau} - \frac{W_H}{KT}\right] \quad (4)$$

This relation implies that the distance (R) depends on temperature (T) and so the exponent (n) is also temperature dependent.

Temperature dependence of conductivity for different salt and ferrite rations are shown in Fig. 10. The sharp change in conductivity at ~70°C may be due to crystalline to amorphous phase transition. The ln σ vs. 1/T plots are Arrhenius before and after the phase transition. The

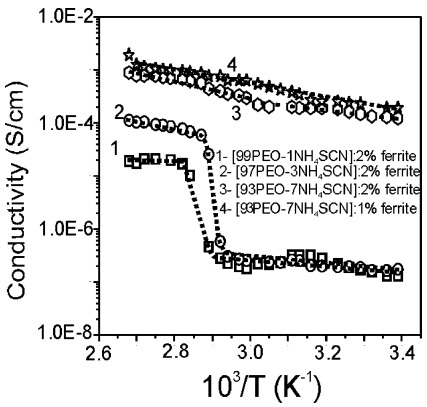

Fig. 10 Variation of electrical conductivity with temperature for different compositions calculated from Cole-Cole plot

Arrhenius type thermally activated process is described by the relation:

$$\sigma = \sigma_o \exp(-E_a/KT) \quad (5)$$

where E_a is the activation energy and σ_0 is the pre exponential factor. The calculated values of these parameters for best conducting nano-composite polymer electrolyte is E_a=0.7 eV, σ_0=2×10^{-4} S/cm (before transition) and E_a=0.2 eV, σ_0=8×10^{-4} S/cm (after transition). The activation energy is lower in amorphous region as compared to the semi crystalline region [38]. The incorporation of ferrite filler tries to reduce the gap or provide the conducting domain for the conduction of mobile charge carriers. The change in conductivity with increasing ferrite content is not very prominent up to 3 wt%, beyond which the segregation of ferrite particles were observed visually. This segregation is due to non complexation of filler with polymer salt matrix.

4 Conclusions

The experimental studies through XRD, SEM, IR and electrical conductivity show that the Al–Zn ferrite nano-filler changes the physical and morphological behaviour of nano-composite electrolyte. Optical investigations reveal the spinodal decomposition structure of the films. XRD and SEM observations confirm formation of nano-composite system with crystallite size varying in between 40 to 60 nm. The electrical conductivity is enhanced by ~4 orders upon dispersion of ferrite and which also controls the gap of crystalline and amorphous conductivity. The accommodation of filler depends on salt content present in the polymer electrolyte.

References

1. D.W. Schaefer, R.S. Justice, Macromolecules **40**, 8501 (2007)
2. Q.H. Zeng, A.B. Yu, G.Q. (Max) Lu, D.R. Paul, J. Nanosci. Nanotechnol. **5**, 1574 (2005)
3. J.H. Koo, *Polymer Nanocomposites: Processing, Characterization, and Applications* (McGraw-Hill Professional, 2006), pp.9–51.
4. Y.D. Premchand, M.L. Divone, P. Knauth, in *Nanocomposites: Ionic Conducting Materials and Structural Spectroscopics*, eds. by P. Knauth, J. Schoonman (Springer, New York, 2008), p. 71.
5. R.C. Agrawal, G.P. Pandey, J. Phys. D.: App. Phys. **41**, 223001 (2008)
6. L.M. Bronstein, in *Metal-Polymer Nanocomposites*, ed. by L. Nicolais, G. Carotenuto (Wiley, 2005), p. 123.
7. K. Pandey, M.M. Dwivedi, M. Tripati, M. Singh, S.L. Agrawal, Ionics **14**, 515 (2008)
8. A. Chandra, P.K. Singh, in *Electroactive Polymers Vol. 1*, eds. by N. Khare, S.A. Hashmi, A. Chandra, A. Chandra, S Chandra (Allied Publishers Pvt Ltd, New Delhi, 2007), p. 80.
9. P.K. Shukla, S.L. Agrawal, Ionics **6**, 312 (2000)
10. F. Croce, R. Curini, A. Martinelli, L. Persi, F. Ronci, B. Scrosati, R. Caminiti, J. Phys. Chem. B **103**, 10632 (1999)
11. S. Rajendran, M. Sivakumar, R. Subadevi, N.-L. Wu, J.-Y. Lee, J. Appl. Polym Sc. **103**, 3950 (2007)
12. A.A. Mostafa, G.A. El-Shobaky, E. Girgis, J. Phys. D: Appl. Phys. **39**, 2007 (2006)
13. R. Lebourgeois, J.P. Ganne, B. Lloret, J. Phys. IV France **7**(Suppl. C1), 105 (1997)
14. S. Gangopadhyay, G.C. Hadjipanayis, B. Dale, C.M. Sorenson, K.J. Klabunde, V. Papaefthymiou, A. Kostikas, Phys. Rev. B **45**, 9778 (1992)
15. M.C. Sable, B.K. Labde, N.R. Shamkuwar, Bull. Mater. Sci. **28** (1), 35 (2005)
16. G. Herzer, M. Vazquez, M. Knobel, A. Zhukov, T. Reininger, H.A. Davies, R. Grossinger, J.L. Sanchez, J. Magn. Magn. Mater. **294**, 252 (2005)
17. R. Iyer, R. Desai, R.V. Upadhyay, Bull. Mater. Sci. **32**, 141 (2009)
18. S.A. Mazen, S.F. Mansour, H.M. Zaki, Cryst. Res. Technol. **38**, 471 (2003)
19. G.P. Joshi, N.S. Saxena, R. Mangal, A. Mishra, T.P. Sharma, Bull. Mater. Sci. **26**, 387 (2006)
20. J. Wang, P.F. Chong, S.C. Ng, L.M. Gan, Mater. Lett. **30**, 217 (1997)
21. S.S. Parkin, N. More, K.P. Roche, Phys. Rev. Lett. **64**, 2304 (1990)
22. O. Yavuz, M.K. Ram, M. Aldissi, P. Poddar, S. Hariharan, J. Mat. Chem. **15**, 810 (2005)
23. K. Na, T.B. Lee, K.-H. Park, E.-K. Shin, Y.-B. Lee, H.-K. Choi, Eur. J. Pharm. Sci. **18**, 165 (2003)
24. Z. Siroma, T. Sasakura, K. Yasuda, M. Azuma, Y. Miyazaki, J. Electroanal. Chem. **546**, 73 (2003)
25. B.D. Cullity, *Element of X-ray diffraction*, 2nd edn. (Anderson-Wesley, London, 1978), pp. 281–286
26. G.K. Williamson, W.H. Hall, Acta Metall. **1**, 22 (1953)
27. T. Araki, Q.T. Cong-Miyata, Q.T. Cong, M. Shibayama, in *Structure and Properties of Multiphase Polymeric Materials* (CRC Press, 1998), p. 233.
28. D.L. Douglass, J. Mat. Science **4**, 130 (1969)
29. L.A. Utracki, *Polymer Bland Hand book Vol-1* (Springer-Verlag, 2002), p. 561.
30. A.E. Bailey, W.C.K. Poon, R.J. Christianson, A.B. Schofield, U. Gasser, V. Prasad, S. Manley, P.N. Segre, L. Cipelletti, W.V. Meyer, M.P. Doherty, S. Sankaran, A.L. Jankovsky, W.L. Shiley, J.P. Bowen, J.C. Eggers, C. Kurta, T. LorikJr., P.N. Pusey, D.A. Weitz, Phys. Rev. Lett. **99**, 205701 (2007)
31. A. Munster, K. Sagel, Z. Electrochem **59**, 946 (1955)
32. R. Bharathi Kannan, A. Chandramohan, J. Chandra Sekar, M.A. Kandhaswamy, Cryst. Res. Technol. **42**, 595 (2007)
33. C. Wickleder, Z. Anorg. Allg. Chem. **627**, 1693 (2001)
34. X.M. Wang, L. Fu, K.C. Zhang, J. Synth. Cryst. **19**, 269 (1990)
35. R.D. Waldron, Phys. Rev. **99**, 1727 (1955)
36. S.T. Hafner, Z. Krist. 115331 (1961).
37. S.A. Mazen, M.H. Abdallah, R.J. Nakhla, H.M. Zaka, J. Mater. Chem. Phys. **34**, 35 (1993)
38. N. Srivastava, A. Chandra, S. Chandra, Phys. Rev. B **52**, 225 (1995)
39. H. Richter, H. Wagner, Solid State Ionics **105**, 167 (1998)
40. A.K. Jonscher, *Dielectric Relaxation in Solids* (Chelsea Dielectric Press, London, 1983), p. 284
41. V. Gupta, A. Mansingh, Phys. Rev. B **49**, 1989 (1994)
42. A.K. Mauritz, Macromolecules **22**, 4483 (1989)
43. S.R. Elliot, Adv. Phys. **36**, 135 (1987)